BEAM RASTER SYSTEM AT CEBAF

C. Yan, J. Beaufait, P. Brindza, R. Carlini
W. Vulcan, and R. Wines
Continuous Electron Beam Accelerator Facility
12000 Jefferson Ave., Newport News, VA 23606

Abstract

A cascade raster system will be used to generate variable rastering pattern on polarized target, cryogenic hydrogen target, and the beam dump with adjustable frequency up to 10 kHz and variable deflection angle from 0.05 mr to 1 mr. Each raster consists of two air-core bedstead coils providing transverse and vertival scans. The magnets are energised by individual MOS power amplifiers being controlled by the scan generator which determines frequency, amplitude, and phase shift between the cascade rasters.

I. INTRODUCTION

A. *Heating effect in the solid target*

Assume that a beam current was 200 μA and the target periphery was kept fixed at the initial target temperature 20 K. The beam spot size is about 0.2 mm diameter. A thin molybdenum target of 2×2 cm^2 was considered. The target thickness was 0.2 mm, which corresponds to about 0.15% radiation lengths (0.204 g/cm^2) for Molybdenum. In this case thermal conduction through the metal target material and the metal frame are considered as the major manner releasing the heat deposited by the beam and the black body thermal radiation can be eliminated. With the beam spot fixed at the center of the target, the steady state beam spot tamperature reached 2500 K. If the beam scans the target with a sinusoidal motion having frequency 100 Hz and amplitude 9.6 mm in one direction, the steady temperature is about 300 K over the target area except the four vertex points of the motion [1]. A further simulation by [2] shows that if a fast two dimensional rastering (f_1 = 2 kHz and f_2 = 0.1176 kHz) is applied to an aluminium target (20 mm × 20 mm). The temperature rise on the target will be quickly saturated at Δt is below 70 K from an initial temperature 300 K after 1 second. For the iron target a temperature rise of 500 K occurs due to the worse termal conductivity and the smaller specific heat.

*This work was supported in part by the U.S. Department of Energy, under contracts No. DE-AC05-84ER40150

B. *Heating effect in the cryogenic target*

In the case of 10 cm liquid hydrogen target operating at 20 K the power dissipation due to the energy loss in the target cell by 200 μA beam is about 1 kW. Along the track of the beam the liquid hydrogen is overheated by the depossited energy of the beam and bubbles will be formed, therefore, a density variation is eventually generated. In order to minimize this bubble formation effect and reduce forced flow velosity to a reasonable level (1 to 10 m/s), the best solution is to makes beam rastering. The global and local beam heating analysis by [3] shows a 18 kHz rastering with 2 mm amplitude is preferable.

C. *Heating effect in the beam dump*

As discused by [4], for an instantanueous spot size of 100 μm, the critical time constant for drilling a hole into the window is 100 μseconds. Also, any window material looses its strength after an energy deposition of 10^{18} ergs/gram by the beam. Therefore, the rastering speed and pattern has to be selected carefully to avoid long dwell times. Tentatively, a spot size of 4×4 cm^2 at the dump was adopted. The spot size at the beam dump entrance can be increased nearly arbitrarily by using high speed magnetic rastering.

D. *Rastering on the polarized target*

The UVa polarised target will have a useful width and height of 2.5 cm. To make full use of it, the rastering of the beam on the target should cover at least 2.5 × 2.5cm^2 [5]. An adjustable offset of rastering current is desirable for the beam alignment. In the polarised target experiment the current density is only 100 nA, it is reasonable to require 1 kHz rastering. The Mϕller polarimeter requires a linear rastering pattern on the iron target with amplitude of 2 mm instead of moving target [6]. The linear scan of the beam will effectively reduce the temperature rise of the target and keep the polarization at an higher level in the beam current range from 10 to 100 μA.

E *Rastering frequency and amplitude*

Parameter	Cryogenic Target	Polarised Targt	Beam Dump materials
Position(m)	146.25	146.25	200.65
Current(μA)	200	0.1	200
Area (cm2)	0.2x0.2	2.5x2.5	4x4
Frequency(kHz)	10-18	0.1-1	0.1
Operation	FR	FR+SR	SR

Table 1: Raster frequency and amplitude, FR:fast raster, SR:slow raster

Design Parameter	SR	FR
Central field (Gauss)	438.8	80.1
Bending angle at 6 GeV	0.84 mr	0.0588
$\int Bdl$ (kG cm)	16.8	1.2
Field Uniformity	10^{-2}	10^{-2}
Effective length (cm)	38.34	15
Physical dimension (cm)	48	25
Inner radius (cm)	1.905	1.27
Number of turns	200	20
Ampere-turns (A-T)	4000	240
Current density (A/cm^2)	148	100
Stored energy (Joules)	6.944	0.0167
Inductance (Henries)	34.7×10^{-3}	84×10^{-6}
DC resistance (Ohm)	0.916	3.02×10^{-3}
RMS power (kW)	2.18	0.528
Type of conductors	Awg 8	Litz
Rastering frequency (Hz)	60	10k

Table 2: Specification of SR and FR magnets

II. Raster Magnet Design by TOSCA

Two bedstead air core coils will be used as the raster magnets. The specification of the coil are listed in Table 2.

The geometry of the raster magnet is shown in Figure 1. The bedstead shape of raster coil will generate a larger uniform field region and keep the high order field components, mainly sextupole component, as small as possible. In order to reach a higher rastering frequency up to 10 kHz, neither iron nor laminate iron material can be used as the raster magnet. Ferrite magnet is also not preferable because its small hysteresis makes difficulty for phase control.

III. Frequency Charasteristics of Raster Coil

A triangle waveform is selected to drive the raster coil. Based on the Fourier theorem, an arbitary function F(x) can be expressed

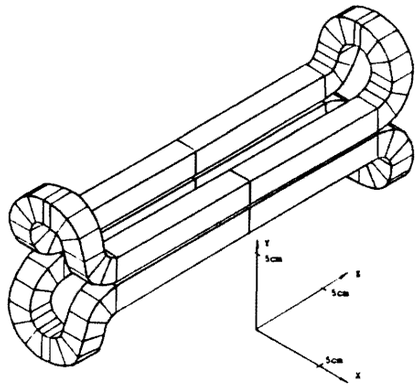

Figure 1: TOSCA layout of FR raster magnet

$$F(x) = \sum_{n=1}^{\infty}[A_n \sin n\omega_n x + B_n \cos n\omega_n x] \qquad (1)$$

Where, $\omega_n = 2\,\pi f_n$, A_n and B_n is the amplitude of n-harmonic components, therefore, the amplitude of the n-harmonic $= \sqrt{A_n + B_n}$ and the intensity of the n-harmonic $= A_n^2 + B_n^2$.

In the case of identical triangle waveform

$$y = \begin{cases} -T - x & -T \le x \le -T/2 \\ x & -T/2 \le x \le T/2 \\ T - x & T - x \le x \le T \end{cases} \qquad (2)$$

The Fourier expension of the triangle waveform is

$$y = \frac{4T}{\pi^2}\sum_{n=1}^{\infty}\frac{(-1)^{n-1}}{(2n-1)^2}\sin\frac{(2n-1)\pi x}{T} \qquad (3)$$

$$y = \frac{4T}{\pi^2}\left[\sin(\frac{\pi x}{T}) - \frac{1}{9}\sin(\frac{3\pi x}{T}) + \frac{1}{25}\sin(\frac{5\pi x}{T}) - ...\right] \qquad (4)$$

Therefore, the ratio of the amplitudes and the intensities of the first, the third, and the fifth harmonic compoenets are $1 : \frac{1}{9} : \frac{1}{25}$ and $1 : \frac{1}{81} : \frac{1}{225}$ respectively.

The 20 kHz triangle waveform generated from Tektronix FG 501A 2 MHz function generator was experimentally analysed by HP network analyser. The frequency spectrum is displayed in Figure 2. The ratio of relative amplitudes of the fundamental frequency, the third and the fifth harmonic is as the same as the computation from Fourier analysis mentioned above.

Losses in a conductor due to eddy currents are nearly all instances the result of a combination of losses due to the skin effect and proximity effect. The skin effect becomes more significant with increasing frequency and wire diameter. The skin effect is a function of the ratio d/Δ, where d is the diameter and Δ is the penetration depth. Penetration depth Δ for copper conductor at 20° is $\Delta = 65.5\sqrt{\ }$

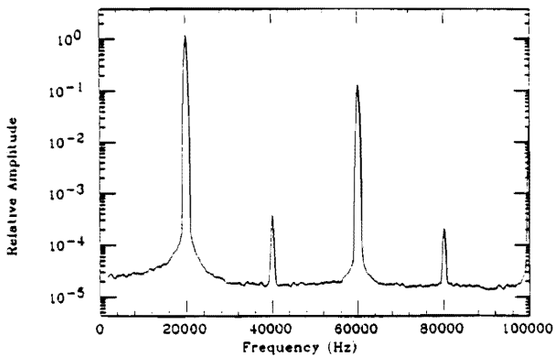

Figure 2: Frequency spectrum of triangle waveform from HP analyser

mm, with f in Hz. At 20 kHz the corresponding penetration depth is 0.463 mm. To judge the resistance increase due to skin effect $R_{AC} = R_{dc} + R_{SE} = R_{dc}(1+F)$. Figure 6 shows (1+F) as afunction of the ratio d/Δ. To avoid from a considerable increase of R_{AC}, it is better to select d/Δ neay unit. Proximity effect is eddy current losses induced by stray alternating magnetic field. When d/Δ is $\leq$ 1, e.g. at low frequency or small diameter wire, the proximity effect is negligible. This is the case that an appropriate diameter Litz wire is selected for the use of the raster windings.

Varies techniques are used in practice to eliminate or reduce the undesired aspects of the skin effect. One can divide the conductor body into pieces insulated from one another of which at least one dimension is smaller than the skin depth. The use of stranded conductors, in the place of solid conductors, when the cross section dimensions are larger than the skin depth. A trabded conductor such as Litz cable consists of a large number of small wires insulated from each other, except at the terminals. The wires are interwoven in such a way that each wire occupies each position in a boundle for approximately the same length of conductor. In this manner, the current is forced to devide equally between the wires, and to be uniformly distributed throughout the cross section of the stranded conductor. The insilation surrounding each wire provides a canal through which power can reach the surface of the wire throughout its length. The radius of each wire must be smaller than the skin depth.

The use of insulated sheets in magnetic cores and the stranding in conductors may be regarded as ways of fabricating materials with anisotropic conductivity. A stack of insulated sheets has appreciable conductivity only in the direction of the laminations, and stranded conductor canducts only in the direction of the wires. For SR raster magnet Litz cable is not neccesary for the winding because at lower frequency 60 Hz the skin depth in copper conductors is 8.5 mm, Awg no. 6 cable can be easily used for

Operating frequency (kHz)	20 - 50
Equivalent AWG	8
Number of strands	660
Strand AWG	36
Outer insulation	nylon wrapped/bare coated
Normal outer diameter (inch)	0.186
LBS/MFT	57.2
D.C. Resistance (Ohm/MFT)	0.697
Construction	5×3×44/36

Table 3: Specification of Litz cable for the windings

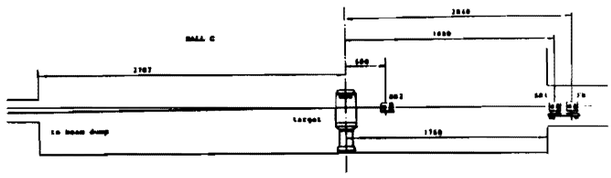

Figure 3: The raster system in Hall C beam line

winding. For the FR raster magneyt, a round Litz cable 660/36 is used to make the winding. The specification is shown in Table 3.

IV. Operational Performance

The raster system is arranged as shown in Figure 3.

A fast raster system (FR) is placed just at the entrance of Hall C - in front of the first chicane magnet (BE). With a bending power 0.0588 mr at 6 GeV/c it is able to provide $2\times$ $2mm^2$ rastering area on the cryogenic target. A combined SR raster system which is located in front of the FR raster scans the beam on the polarized target with rastering area 2.5 × $2.5cm^2$. The second SR raster near the target chamber executes two functions: in the absence of polarized target it scans the beam to a safety size (4×4 cm^2) on the beam dump and in the operation of polarized target it derasters the beam with opposite phase in order to reduce the large ammount background generated from scattered beam at the wall of beam pipes.

Each raster system consists of two pairs of bedstead coils, one for horisontal scan, another for vertical scan. Different rastering patterns have been simulated and compared by two dimensional oscillascopic Lissajous figures. Instead of TV frame/line scan rate the best ratio (1.721) of the two rastering frequency was found, which gives the longest trajectory traversal and fast uniform distribution.

FR raster magnet is driven by PA30 MOS power amplifier (APEX micro technology). PA30 is an ideal driver for FR magnet due to its excellent features of high voltage,

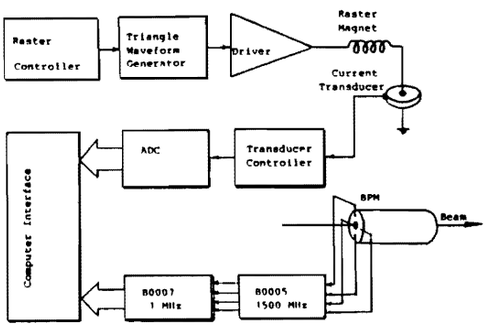

Figure 4: Beam Position Measurement in Raster System

high current, and high internal dissipation. SR magnet is driven by a resonance circuit, which consists of a π-type LC resonance circuits, impedance match network, and low frequency power amplifier. Both of those drivers are under construction.

Ceramic duct should be used as vaccum pipe of FR raster magnet. The ceramic vaccum duct avoids heating-up effect and the field attenuation due to eddy currents induced by alternative magnetic field. A very thin metal coating layer should be applied in the inner-wall of the duct conducting image current produced by beam.

V. Instantaneous Beam Position Measurements

As an auxiliary experimental data in some particular case, for example, the experiment with polarised target, an instantaneous beam position should be measured. In Hall C beam line the BPM in front of the raster could provid an instantaneous beam position information. With a minor modification CEBAF 150 ohm BPM could trace beam position measurement up to 15 kHz. Inside the raster system by placing a current monitor around a current carrying conductor cable of the raster winding, the current monitor will sense the associated magnetic field wothout requiring directly connection. The wide band current monitor converts the primary current into a proportional voltage signal, which is then digitised by ADC module and is sent into data aquisition system as a indication of beam position. A sketch diagram for beam position monitoring system is shown in Figure 4.

Instead of the offset adjustment in raster power amplifier two individual beam correctors placed in the match section of Hall C beam line will be used for beam offset adjustment. Therefore, the raster amplifiers are only operating at AC and the long term reliability of raster system will be great increased.

References

[1] Conceptual Design Report on Basic Experimental Equipment (revised), CEBAF, April 13, 1990

[2] Javer Gomez. Private communication, December 1992

[3] J. Mitchell. Global and Local Beam Heating in the Hall C Cryo Target, CEBAF, March 2, 1993

[4] B. Mecking. C. Sinclair. CEBAF Internal Meeting on Beam Lines to Experimental Area, 28 November, 1992

[5] D. Day and I. Sick. Internal communication - Consideration Concerning Chicane for G_{en}, July 23, 1992

[6] Matthias Loppacher. Progress Report of the CEBAF Hall C Møller Polarimeter, November 1992.